Brittle failure in RC masonry infilled frames: the role of infill overstrength

Gianni Blasi[1,2], Flavia De Luca[*1], Maria Antonietta Aiello[2]

[1]*Department of Civil Engineering, University of Bristol*
Queen's Building, University Walk, Bristol, UK, BS8 1TR
[2]*Department of Innovation Engineering, University of Salento*
Via Monteroni, 73100, Lecce, Italy

SUMMARY

The interaction between an infill panel and a reinforced concrete (RC) column can lead to the brittle failure of the structural element. A novel combination of cutting-edge analytical modelling approaches for masonry infills and RC elements is employed to simulate five experimental tests (three infilled and two bare) characterized by brittle failure modes. The infill is modelled with a multi-strut idealisation, and the RC column is modelled using the recently developed *PinchingLimitStateMaterial* in OpenSees. The effects of the infill type (solid or hollow) and ductility characteristics of the RC elements on the optimal modelling parameters are investigated. The focus of this study is on the assumption of the overstrength ratio between the maximum and cracking strengths of the panel when brittle failure occurs. The preliminary assumption for this parameter is the widely accepted value of 1.3 suggested in the formulation by Panagiotakos and Fardis. This value is found to influence the shear failure simulation. To more accurately predict brittle failure, higher overstrength values of the infill are used in the numerical model to improve the matching between the numerical and experimental tests. These values are then compared with the approximate estimation of the overstrength ratio from a database of 98 experimental tests. The suggested estimation of the overstrength ratio is systematically greater than 1.3 and dependent on the infill type (i.e., 1.44 for hollow and 1.55 for solid infills). The proposed values can have a high impact on future code-compliant recommendations aimed at verifying the likelihood of the occurrence of brittle failure in columns due to their interaction with infill panels.

KEYWORDS: masonry infilled reinforced concrete frame; experimental tests; equivalent strut model; shear failure; infill overstrength.

1. INTRODUCTION

"Infilled frame structural systems have resisted analytical modelling." as reported in the bulletin 231 by the Comité Euro-international du Béton (CEB 1996) and originally stated by Axley and Bertero (1979) in 1979. In the last two decades, the scientific community has made significant progress on both experimental and analytical aspects of this problem. On the other hand, the influence of infill on the seismic behaviour of reinforced concrete (RC) frames is still a focus of the earthquake engineering community, and its relevance has been continuously evidenced by structural damage observations after earthquakes (e.g., Sezen et al. 2003; Decanini et al. 2004; Çelebi et al. 2010; Verderame et al. 2011; Manfredi et al. 2014; De Luca et al. 2017).

Considering the significant increase in the global strength and stiffness of RC frames due to the presence of infill, existing building codes address this issue by introducing design recommendations and simplified formulations to encourage the evaluation of the influence of the panel on the structural performance as common practice (e.g., FEMA 356 2000; EN 1998-1 2004; ASCE/SEI 41-13 2014). In ASCE/SEI 41-13 (2014) and FEMA 356 (2000), considerable attention is paid to the local interaction between the panel and surrounding frame; according to these codes, the required shear strength of the column should be evaluated in terms of the lateral strength of the infill.

In Eurocode 8 Part 1 (EN 1998-1 2004), an additional shear demand in the column is prescribed to account for the local interaction with the infill panel. Along the contact length between the infill and column, the shear strength of the column should be considered the minimum value between the lateral strength of the panel and the shear demand determined from the capacity design approach.

Previous studies already evidenced how the failure mode of the frame can be significantly modified due to the presence of the panel (e.g., Pujol and Fick 2010), particularly in the case of existing buildings (e.g., Dolšek and Fajfar 2005; De Luca et al. 2014; Perrone et al. 2017). Although the inter-storey displacements are reduced (Hak et al. 2012; Ricci et al. 2016), the increase in stiffness generally leads to a higher seismic demand on the frame members (Dolšek and Fajfar 2008; Perrone et al. 2016). Furthermore, post-earthquake damage observations highlight how the brittle failure of columns is often caused by the increase in stresses locally transferred from the panel to the column.

[*]Corresponding author

Numerous studies were conducted on different types of infilled frames to provide simplified analytical models to evaluate the forces transferred to the frames, depending on the failure mode of the infill (e.g., Mehrabi et al. 1996; Colangelo 2005; Cavaleri and Di Trapani 2014; Noh et al. 2017). At the onset of damage in the panel, a strut mechanism occurs due to the migration of the stresses to the diagonal zone, and stresses at the interface between the corners of the panel and the frame members increase. Experimental studies on the local interaction between frames and masonry panels showed that, in the case of poor transverse reinforcement of the columns, early shear failure can occur due to the presence of the infill (Al-Chaar et al. 2002; Basha and Kaushik 2016; Verderame et al. 2016).

Based on the experimental observations, different analytical models were derived in the literature to consider the effect of the infill panel on the response of RC frames under lateral loads. Many numerical analyses aimed at simulating the local interaction phenomena through micro- and macro-modelling approaches (e.g., Stavridis and Shing 2010; Jeon et al. 2015; Ning et al. 2017). The equivalent truss macro-model, originally proposed by Polyakov (1960), is one of the most commonly adopted models in numerical and analytical studies. Various configurations of this approach have been proposed in the literature, depending on the number of trusses adopted and their mechanical properties (e.g., Chrysostomou et al. 2002; Varum et al. 2005; Crisafulli and Carr 2005).

Generally, the mechanical behaviour of the equivalent strut is evaluated by considering the properties of both the frame members and infills. The number of trusses adopted in the model highly modifies the local interaction phenomena. It was already determined that multi-truss models are the best macro-modelling option for investigating the local interaction between panels and frames (e.g., Asteris et al. 2011; Verderame et al. 2011; Burton and Deierlein 2013), while single-truss models are generally used in global analyses (Kose 2009; Perrone et al. 2016).

The presence of infills can lead to the brittle failure of frame members, especially in the case of poor seismic details. Thus, an accurate evaluation of the mechanical and geometrical properties of the infills must be conducted to more accurately simulate the actual behaviour of the system and to predict the potential occurrence of the brittle failure.

Analytical models provided for evaluating the nonlinear behaviour of infill are generally characterized by a piecewise linear force-displacement relationship. This relationship is composed of an elastic slope before the panel cracks, followed by a hardening slope and a post-peak softening behaviour, representing the degradation of the panel before failure.

According to experimental results, different analytical formulations are available in the literature to define the strength of the panel for each failure mode considered (Bertoldi and Decanini 1993; Mehrabi et al. 1994; Chrysostomou and Asteris 2012); nevertheless, general formulations (i.e., avoiding the specific identification of the failure mechanism) are often preferred for predictive studies, in which the failure mode of the panel is unknown or not easily predictable (e.g., very similar values of the limit forces are predicted for different failure mechanisms and the determination of the failure mode is highly uncertain).

Herein, a numerical model is developed to simulate the results obtained from experimental tests on different types of infilled frames and to reproduce the failure mode of the frame, focusing on the shear failure of the column. Experimental tests in which brittle failure occurred have been selected from the literature, with the aim of covering different infill types (solid and hollow) and different design approaches for the RC frames (non-ductile and ductile). Five experimental tests are considered (Mehrabi et al. 1996; Basha and Kaushik 2016; Verderame et al. 2016): two bare and three fully infilled. Four of these tests have never been modelled numerically in an effort to match the cyclic behaviour.

A three-strut equivalent model is adopted to simulate the presence of the infills. The mechanical properties are defined according to the widely used and consolidated formulation proposed by Panagiotakos and Fardis (Panagiotakos and Fardis 1996). In the original formulation, the maximum strength developed in the panel is related to the cracking strength through an overstrength ratio that is assumed to be 1.3. The influence of this parameter on the numerical simulation is analysed by adopting various overstrength ratios and comparing the numerical and experimental results. Moreover, to assess the reliability of the proposed approach, a wider study on the overstrength factor is proposed; 98 experimental tests on infilled frames are selected from a previously assembled database (De Luca et al. 2016) to calculate the overstrength factors as metadata through a simplified procedure. This approach allows a comparison of the overstrength factors resulting from the analytical-experimental investigations and those obtained from the database, to assess the optimal values as a function of the infill type and structural design of the RC members. The overstrength factors obtained are systematically greater than 1.3 and equal 1.44 for hollow clay bricks and 1.55 for solid bricks, confirming the trend obtained in the numerical simulations. This result can have applications in the approximate assessment formulations to be implemented in the codes. The different effect of the solid and hollow infills has been well documented in the literature for a long time (CEB 1996), but it is a more recent trend to provide specific

recommendations for solid and hollow infills, as has been done recently for the empirical fragility functions of infills (e.g., Sassun et al. 2016).

2. ANALYTICAL MODELLING OF LOCAL INTERACTION AND BRITTLE FAILURE

The damage observed after recent earthquakes evidenced the considerable influence of infill on the failure mechanism of RC frames. In many cases, the presence of the panel led to the shear failure of the columns, due to the increase in the stresses at the interface between the frame and infill. The mechanical properties of the panel are recognized as important parameters influencing this phenomenon (e.g., Dolšek and Fajfar 2001; Verderame et al. 2011), particularly in the case of lightly shear-reinforced columns (Sezen et al. 2003; Sezen and Moehle 2004), as reported in Figure 1.

(a) (b)

Figure 1. Column shear failure in RC infilled buildings in Italy (a) after the 2012 Emilia earthquake (Parisi et al. 2012) and (b) after the 2016 Central Italy earthquake (De Luca et al. 2017).

2.1 Infill macro-model

Most of the experimental studies performed in the last few decades investigated the response of infilled frames both in terms of their global and local behaviour. The main failure modes that characterize the response of the specimens as soon as the static load increases have been widely analysed in the tests performed by Mehrabi et al. (1996) on 1:2 scaled single-bay, single-storey infilled frames.
In the first elastic phase, the panel acts as a monolithic element, and the behaviour is dependent on the interface condition between the panel and surrounding frame. By increasing the lateral load, the first cracks in the infills lead to separation from the frame, and a compression strut mechanism occurs. In the experimental campaign carried out by Mehrabi et al. (1994), four mechanisms were identified in the masonry infilled frames, depending on the mechanical properties of the masonry and on the relative panel-to-frame stiffness. Figure 2 graphically shows the main failure modes identified by Mehrabi et al.: (1) mid-height cracking, (2) diagonal cracking, (3) horizontal slip and (4) corner crushing.

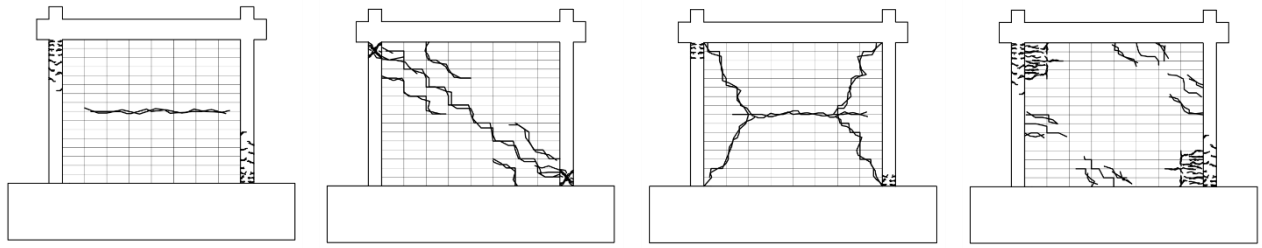

(a) (b) (c) (d)

Figure 2. Failure mechanisms of infills (a) mid-height sliding, (b) diagonal cracking, (c) bed joint sliding, and (d) corner crushing.

The equivalent truss approach can reliably simulate the behaviour of infilled RC frames and investigate the local interaction between the frame and panel. The approach proposed by Bertoldi and Decanini (1993) provides four different formulations to evaluate the compressive strength of the diagonal strut (σ_{br}), depending on the expected failure mechanism (diagonal cracking, horizontal sliding, corner crushing or diagonal crushing), mechanical properties of both the brick units and mortar joints and vertical load on the panel. On the other hand, the definition of the failure mode is often challenging, leading, in many cases, to underestimation of the actual strength of the panel (e.g., Uva et al. 2012; Burton and Deierlein 2013; Jeon et

al. 2015). Since the present work is aimed at providing an accurate but simplified method to capture the shear failure of the column, the correct approach should focus on the accurate estimation of the lateral strength of the panel instead of the accurate prediction of the failure mode.
The formulation adopted in the present work, proposed by Panagiotakos and Fardis (1996), is still widely employed in many analytical studies due to its accuracy in matching experimental data from in-plane tests (e.g., Noh et al. 2017), providing more realistic estimations of the response of a panel in terms of strength. The response of the equivalent strut model is defined through a piecewise linear load-displacement behaviour, depending on the mechanical properties of the panel and the surrounding frame. The initial stiffness of the panel (K_1) is calculated by using Equation 1, in which G_W is the tangent modulus of the infill and L_W, t_W and h_W are the length, thickness and height of the panel, respectively.

$$K_1 = \frac{G_w t_w L_w}{h_w} \tag{1}$$

The first cracking strength F_{cr} is evaluated as the product of the shear strength of the panel τ_w, obtained from diagonal compression tests according to ASTM E 519-02 (2002), and the cross section $A_w = L_w \cdot t_w$.
Equation 2 is adopted to evaluate the post-cracking hardening stiffness (K_2), depending on the width of the equivalent truss section (b_W), Young's modulus (E_W), and the diagonal length (d_w) of the panel.

$$K_2 = \frac{E_w b_w t_w}{d_w} \tag{2}$$

The analytical formulation provided by Stafford Smith and Carter (1969), later introduced in FEMA 306 (1998), is used to evaluate the relative panel-to-frame stiffness (Equation 3).

$$\lambda = \sqrt[4]{\left(\frac{E_w\, t_w\, sin(2\theta)}{4EIh_w}\right)} \tag{3}$$

In Equation 3, θ is the angle of the diagonal dimension of the panel, while E and I are the Young's modulus of the concrete and the moment of inertia of the cross section of the RC frame columns.
Mainstone (1971) provided Equation 4 to evaluate the width of the diagonal zone of the panel where the strut mechanism develops (b_w). This relation was also introduced in FEMA 274 (1997) and FEMA 356 (2000) and then adopted in several studies focusing on the influence of infill on the lateral behaviour of RC frames (e.g., Dolšek and Fajfar 2008).

$$\frac{b_w}{d_w} = 0.175\lambda {h_w}^{-0.4} \tag{4}$$

The peak shear strength at the end of the hardening branch F_m is equal to $1.3F_{cr}$, while the softening slope is evaluated as a proportion of the initial elastic stiffness. The results obtained from the experimental tests on infilled frames showed that the softening stiffness (K_3) was in the range $0.005K_1 \leq K_3 \leq 0.1K_1$ (Crisafulli 1997). In the present study, a good match was obtained with all the experimental results assuming a softening stiffness value equal to $0.02K_1$.
Several single- and multi-strut macro-models are provided in the literature. Since the adoption of a single truss generally leads to an inaccurate estimation of the shear forces in the columns, these models are mostly used to conduct global analyses (Crisafulli et al. 2005). Multi-truss approaches are preferred to investigate the local interaction, since the total stiffness of the panel is distributed among the trusses (Chrysostomou et al. 2002; Verderame et al. 2011; Burton and Deierlein 2013; Jeon et al. 2015) and a better estimation of the shear in the column can be obtained.

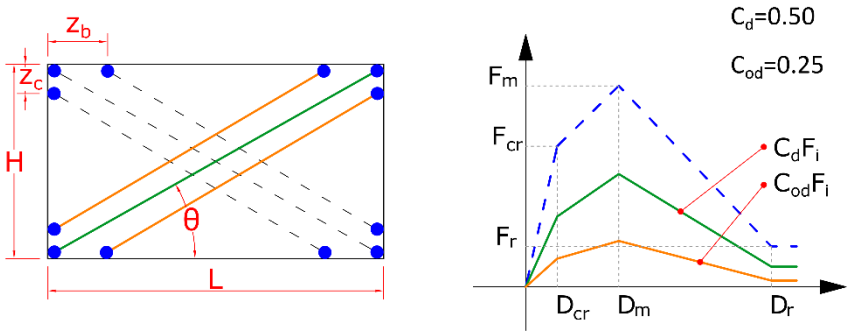

Figure 3. Description of the model proposed by Chrysostomou et al. (2002).

In this study, a finite element model is proposed and developed in OpenSees (McKenna et al. 2000) with the aim of evaluating the response of RC infilled frames under cyclic loading. The infill panel is modelled by adopting the three-strut approach (Figure 3) proposed by Chrysostomou et al. (2002) to more accurately reproduce the local effect due to the frame-infill interaction. The global stiffness of the panel is distributed among the three elements by assigning 50% of the total stiffness to the central truss and 25% to each of the off-diagonal trusses, according to the original model proposed by Chrysostomou (1991) and later employed in different numerical studies (El-Dakhakhni et al. 2003; Verderame et al. 2011).
The location of the off-diagonal trusses is defined by adopting the approach proposed by Al-Chaar (2002), using two non-dimensional parameters (C_d and C_{od}) representing portions of the width b_w (Equation 2) assigned to each strut. In Equations 5 and 6, the calculated distances of the columns and beams from the joints are provided. Following the stiffness distribution, the coefficients C_d and C_{od} are equal to 0.50 and 0.25, which are assigned to the central and the off-diagonal struts, respectively (as per Figure 3b).

$$z_c = \frac{C_d b_w + C_{od} b_w}{2cos\theta} \tag{5}$$

$$z_b = \frac{C_d b_w + C_{od} b_w}{2sin\theta} \tag{6}$$

Despite the reliability and simplicity of the model proposed by Panagiotakos and Fardis, some authors noted that the formulation to evaluate the peak strength of the infill F_m should be adapted to obtain a better fit to experimental results. In the study conducted by Burton and Deierlein (2013), the results from 14 experimental tests on infilled RC frames were used to determine the equivalent strut parameters, which were compared to the results of existing analytical models. The results obtained suggested that the ratio F_m/F_{cr} ranged from 1.2 to 1.6, with a mean value equal to 1.4. Numerical studies on the local interaction between a frame and infill must consider an *ad hoc* overstrength of the panel, especially when this feature is crucial to determine the brittle mechanisms of the shear failure of the columns (e.g., in case of poor seismic detailing of the columns).
In the present study, the calibration of parameters defining the force-displacement response of the equivalent strut is proposed, with the aim of providing a numerical model that can predict the shear failure of columns from knowledge of the presence of infill and infill type (i.e., solid or hollow). In most of the experimental studies conducted on infilled frames, shear failure of the columns occurred with panels made of solid bricks (e.g., Mehrabi et al. 1996; Basha and Kaushik 2016) whose higher compressive strength influenced the lateral strength of the infill. According to the formulation provided by the codes (e.g., FEMA 356 2000; EN 1996-3 2006), the parameters influencing the lateral strength of the panel are the compressive strength of the bricks and the shear strength of the mortar bed joints; thus, an accurate evaluation of these properties should be made to characterize the properties of the panel and to more accurately estimate the shear failure of columns due to local interaction. Moreover, the failure mode of the infill influences the stress transferred along the contact zone between the column and panel. According to the existing literature, the shear failure of columns often occurs after diagonal cracking of the panel (Mehrabi et al. 1996; Basha and Kaushik 2016; Verderame et al. 2016), which increases the force transferred at the columns ends.
According to this assessment, the present study focuses on experimental tests in which diagonal cracking of the panel occurs, considering two different types of panels (hollow and solid bricks) and evaluating the influence of the transverse reinforcement of the columns.

In the original model by Panagiotakos and Fardis, the hysteretic behaviour of the panel is defined by the parameters α, β and γ (Figure 4a). In the unloading phase, the stiffness K_u is equal to the elastic stiffness K_1, until the force reaches the value βF_m. At this stage, pinching occurs due to the closure of the cracks, leading to a stiffness reduction until βF_m is attained in the opposite direction. The displacement at the end of the pinching phase is defined by shifting the elastic displacement $\beta F_m/K_1$ by the value $\gamma(D_i-D_{cr})$, where D_i is the maximum displacement obtained in the considered direction during the loading history.
The reloading stiffness $K_{r,i}$ is defined by constraining the intersection between the unloading branch (from the point $[F_i; D_i]$) and the reloading branch to be at a force level equal to $F_i(1-\alpha)$. A calibration of the parameters α, β and γ was carried out in the study by Panagiotakos and Fardis (1996), based on the results of experimental tests on infilled RC frames provided in the literature. The best fit of the experimental results was obtained with values of α=0.15, β=0.1 and γ=0.8.

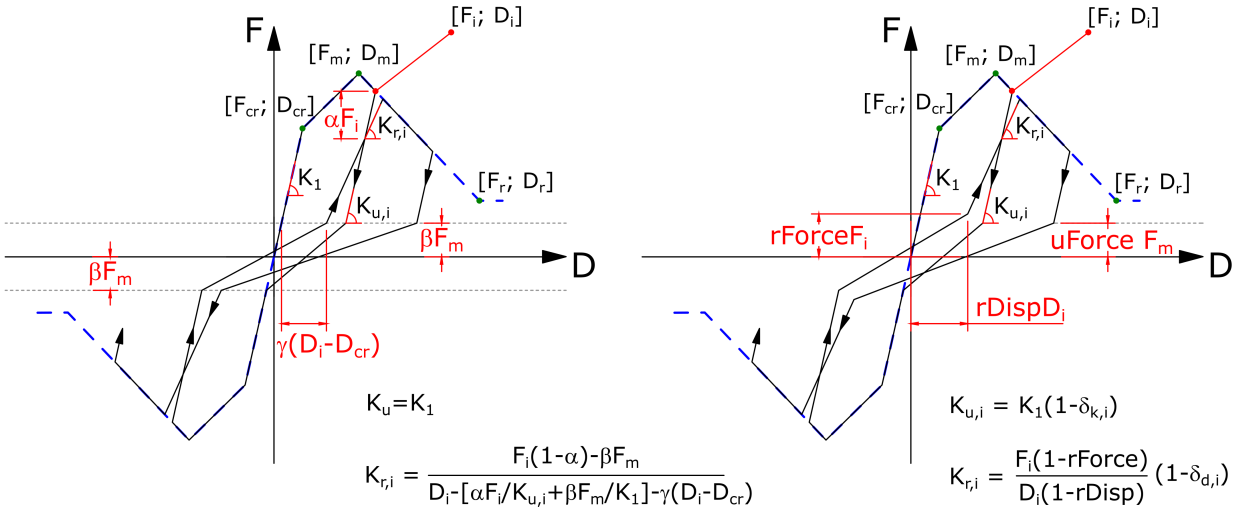

Figure 4. Comparison between the hysteretic model (a) by Panagiotakos and Fardis and (b) the *Pinching4* model available in OpenSees.

In our finite element model of the infill, *Pinching4* material is used to define the hysteretic behaviour of the trusses (Figure 4b). Near-zero values for the definition of the tensile backbone curve of the uniaxial material are adopted to obtain compression-only elements. The starting point of the pinching branch, in the *Pinching4* material, is determined by the ratio between the strength developed upon unloading and the maximum strength F_m (uForce), while the reloading phase begins at the point [rForce·F_i; rDisp·D_i]. The strength and stiffness degradation due to cyclic loading are defined in the model, according to Equation 7, which was provided by Lowes et al. (2003).

$$\delta_{par} = \alpha_{1,par} \cdot \left(\frac{D_i}{D_{collapse}}\right)^{\alpha_{3.par}} + \alpha_{2,par} \cdot \left(\frac{E_i}{E_{mono}}\right)^{\alpha_{4,par}} \leq D_{lim} \quad (7)$$

In Equation 7, δ_{par} is the damage index of the considered parameter (i.e., δ_k for stiffness and δ_d for displacement, as shown in Figure 4b), whose maximum value D_{lim} is user-defined. $D_{collapse}$ is the displacement at failure, E_i is the energy dissipated from loading, E_{mono} is the energy of a monotonic pushover to the residual shear strength, and $\alpha_{i,par}$ are non-dimensional coefficients.
Kumar et al. (2015) proposed a calibration of the parameters of the *Pinching4* material to simulate the cyclic behaviour of the panel in RC infilled frames. They employed 35 experimental tests on single-bay, single-story specimens to define the backbone curve, while two different sets of hysteretic parameters (referred to "weak" and "strong" infills, respectively) have been defined using the tests performed by Kakaletsis and Karayannis (2008).
Since uForce and rForce can be equated to β in the model by Panagiotakos and Fardis, for both parameters, the value 0.1 was adopted in the present study, assuming δ_k = 0. Referring to the rDisp and δ_d, no correlation could be found with γ and α; thus, the parameters proposed by Kumar et al. are adopted. Furthermore, since the present study focuses on the calibration of the overstrength ratio F_m/F_{cr}, as well as its role on the failure mode of the column, no cyclic strength degradation was assumed for the infills. This approach allows to obtain

the same results in terms of the lateral strength whether the load application is cyclic or monotonic, according to the modelling approaches adopted in previous studies (Jeon et al. 2015; Burton and Deierlein 2013).

2.2 RC frame model

The brittle mechanism characterized by shear failure of the columns is often due to the presence of infills and significantly affects the structural performance of RC buildings. Based on a database of 51 laboratory tests, Sezen and Moehle (2004) provided a formulation to evaluate the shear capacity of lightly reinforced columns (Equation 8); this formulation was subsequently implemented in ASCE/SEI 41 (2014).
To define the behaviour of columns characterizing buildings with poor seismic details, the database was composed of tests on columns satisfying different selection criteria; specifically, the mechanical transverse reinforcement index ($\rho'' \cdot f_{yt}/f_c$) is in the range $0.01 < \rho'' \cdot f_{yt}/f_c < 0.12$.
In Equation 8, k is a ductility factor varying within the range [0.7;1], while A_t, f_{yt}, and s are the cross section, yielding strength and spacing of the transversal reinforcement, respectively. Additionally, A_g and d are the cross section and effective depth of the column, f_c is the compressive strength of the concrete, and N_{ed} is the axial load.

$$V_n = k\frac{A_t f_{yt} d}{s} + k\left(\frac{0.5\sqrt{f_c}}{\frac{a}{d}}\sqrt{1+\frac{N_{ed}}{0.5\sqrt{f_c}A_g}}\right)0.8A_g \tag{8}$$

After the shear strength is attained, a gradual reduction of the axial load capacity of the column is observed; thus, the post-peak softening behaviour characterizing the load-displacement response of the column can be defined with a displacement capacity approach. 50 of the 51 tests selected by Sezen and Moehle were considered by Elwood and Moehle (2005) to provide a formulation to evaluate the drift at shear failure Δ_s/L and axial failure Δ_a/L. An alternative formulation was introduced by Zhu et al. (2007), based on a database of 125 experimental tests. Their formulation was defined by adopting the same criteria followed by Elwood and Moehle (2005) and by considering a wider range of geometrical transverse reinforcement ratios ($0.0006 < \rho'' < 0.022$). Zhu et al. provided a probabilistic approach to evaluate the drift at shear and axial failure; the drift is calculated from non-dimensional parameters with normal and log-normal probability density functions. A summary of the formulations proposed by Elwood and Moehle and Zhu et al. for the shear and axial failure drift capacities are reported in Table 1. In these formulations, ν is the nominal shear stress, L is the height of the column, and θ_c is the critical crack angle, which is assumed to be 65°.

Table 1. Formulations by Elwood and Moehle and Zhu et al. to evaluate drift at shear and axial failure.

	(Elwood and Moehle 2005) – 50 Tests	**(Zhu et al. 2007) – 125 Tests**
Δ_s/L	$\frac{3}{100}+4\rho''-\frac{1}{40}\frac{\nu}{\sqrt{f_c}}-\frac{1}{40}\frac{N_{ed}}{A_g f_c}\geq\frac{1}{100}$	$0.202\cdot\rho''-0.025\frac{s}{d}+0.013\frac{a}{d}-0.031\frac{N_{ed}}{A_g f_c}$
Δ_a/L	$\frac{4}{100}\frac{1+(tan\theta_c)^2}{tan\theta_c+N_{ed}\left(\frac{s}{A_t f_{yt} d_c tan\theta_c}\right)}$	$0.184exp\left(-1.45\frac{\frac{N_{ed}}{A_t f_{yt} d_c/s}-1}{\frac{N_{ed}}{A_t f_{yt} d_c}\frac{1}{tan\theta_c}+tan\theta_c}\right)$

In our model, the shear behaviour of the columns is defined by using zero-length elements composed of three springs connected in series, placed at the top and bottom of the columns (Figure 5). The first flexural spring behaves linear elastically and is calibrated according to the formulation proposed by Elwood and Eberhard (2010), to consider the bar slip influence on the flexural stiffness of the column.
To simulate the behaviour of columns characterized by shear failure due to lateral loading, Leborgne and Ghannoum (2014) proposed a finite element model (*Pinching Limit State Material*) developed in OpenSees (McKenna et al. 2000); the shear failure is controlled through displacement- and force-dependent parameters that can be user-defined or evaluated automatically on the basis of the properties of the columns.
The *Pinching Limit State Material* model (Leborgne and Ghannoum 2014), in its user-defined option, is adopted in our finite element model to monitor shear in the column and to define the hysteretic response of the shear springs after failure. The behaviour of the shear spring is characterized by a linear elastic slope (K_{shear}) until the shear strength of the column is reached and is evaluated with Equation 8. According to the approach proposed by Elwood (2004), the softening stiffness of the column ($K_{deg,s}$), after the shear strength is reached, is calculated from the equation $K_{deg,s} = V_n/(\Delta_a-\Delta_s)$. This formulation is obtained from the assumption that once

the displacement at axial failure Δ_a is achieved, the shear strength of the column drops to zero, as reported by Nakamura and Yoshimura (2002).
The axial springs are defined by adopting the *Axial Limit State* material (Elwood 2004). According to Reza and Kakavand (2009), the elastic stiffness of the spring K_{axial} is evaluated as EA_g/L, while the softening stiffness of the column after axial failure ($K_{deg,a}$) is defined as $-0.02EA_g/L$.
To consider the influence of the axial load on the response of the frame, a fibre-based distributed plasticity approach is adopted to model the beams and columns. *Concrete02* and *SteelMPF* materials are used for the concrete and reinforcing steel; alternatively, equivalent results are obtained by adopting *Hysteretic* material for the reinforcing steel, as done in previous studies (Jeon et al. 2015; Reza and Kakavand 2009). Analytical formulations proposed by Mander et al. (1988) are used to define the stress-strain relationships of the confined and unconfined concretes, while the steel behaviour are modified to consider the cyclic compressive strength degradation due to buckling, according to Dhakal and Maekawa (2002).
In addition to the force-based approach, the model proposed by Leborgne and Ghannoum (2014) also includes a displacement-based shear detection, which is performed by defining a chord rotation limit (i.e., rotLim parameter in the model). Leborgne and Ghannoum identified the main parameters influencing the rotational capacity of columns characterized by shear failure after flexural yielding based on experimental results for the evaluation of the rotation across the plastic hinge at shear failure.

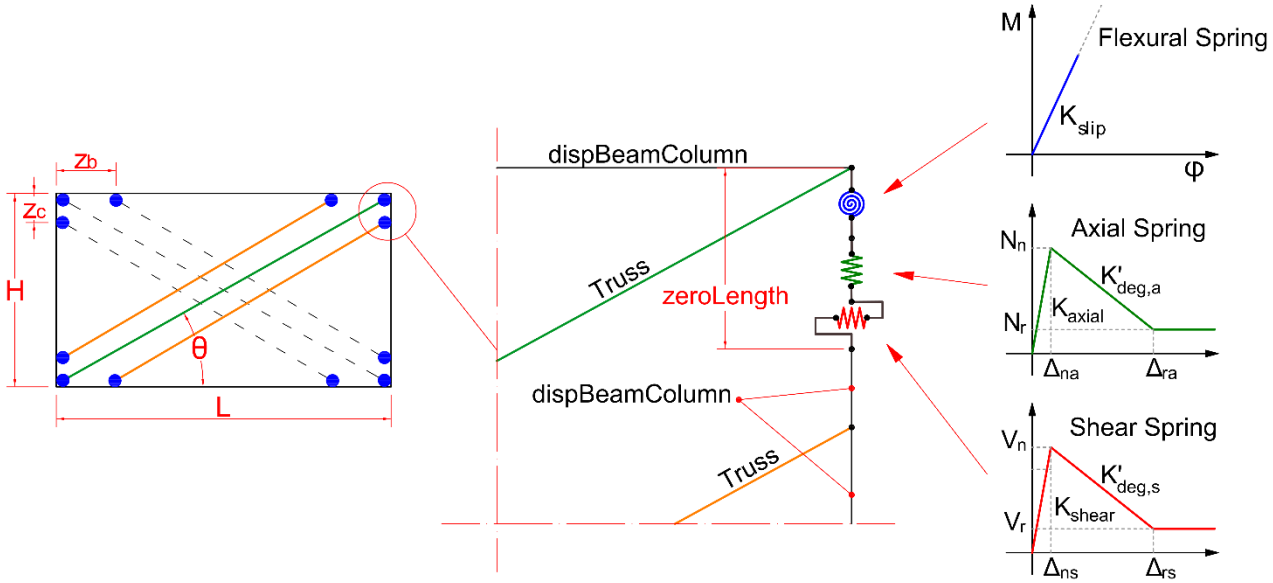

Figure 5. Description of the finite element model adopted for the RC frame.

Herein, a preliminary study of the influence of the assumed rotLim value is conducted on the experimental test by Sezen and Moehle (2004). Zhu et al. (2007) compared the empirical Δ_s with the measured $\Delta_{s,test}$ from the tests. They showed that the rate $\Delta_{s,test}/\Delta_s$ has a mean value equal to 1.03 and a coefficient of variation (COV) equal to 0.35. Considering a normal distribution, the 15th, 50th, and 85th percentiles (i.e., Δ_{s15} = 0.016, Δ_{s50} = 0.027 and Δ_{s85} = 0.038) are considered for Δ_s in the simulation of the experimental test conducted by Sezen and Moehle (2004).
For Δ_{s15}, the corresponding shear strength in the column V(Δ_{s15}) is lower than V_n, thus, an underestimation of response in terms of strength is obtained and the brittle failure prediction occurs earlier with respect to the test, as reported in Figure 6a. On the other hand, for Δ_{s50} and Δ_{s85}, V(Δ_{s50}) and V(Δ_{s85}) are higher than V_n. Shear failure is predicted due to the attainment of the maximum strength; additionally, even if the response of the element is underestimated in terms of drift capacity, the simulation more closely matches the experimental results (Figure 6b).
It is worth noting that the value of the rotation limit resulting from Equation 9 by Leborgne and Ghannoum (i.e., rotLim = 0.014) is lower than both the median obtained value from the formulation provided by Zhu et al. (rotLim = 0.027) and the value obtained by Elwood and Moehle (2005) (rotLim = 0.024).
The intended application of the model proposed herein is to analytically identify the cases of shear failure induced by local interaction with the infill. A shear failure caused by drift does not highlight the difference between infilled and bare frames and provides less-useful results for the simplified code-oriented evaluations of local infill demand on the column. Based on the above considerations, the value of Δ_{s50} obtained by using

the approach of Zhu et al. is the most suitable option for rotLim in the model developed in this study and is consistently adopted in section 3.

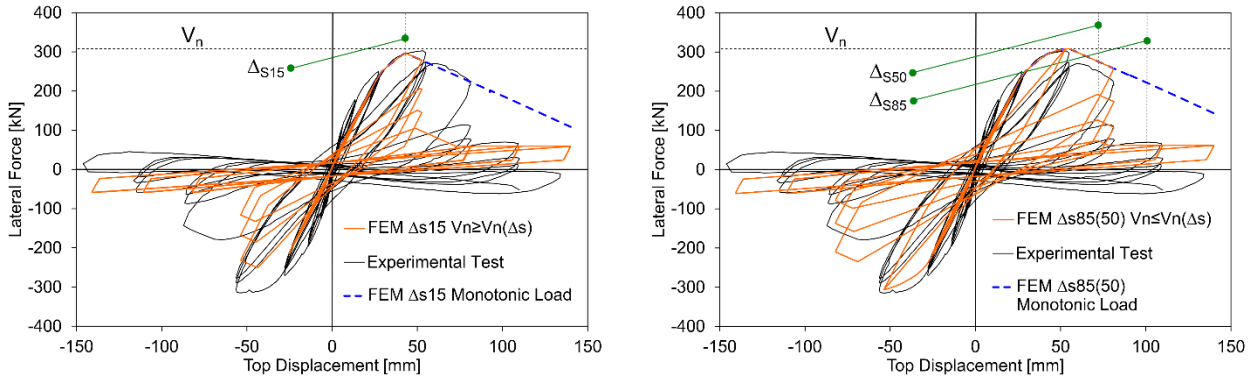

(a) (b)

Figure 6. Effect of rotLim on shear failure detection from monotonic (dotted line) and cyclic (solid line) responses for (a) rotLim=Δ_{s15} and (b) rotLim = Δ_{s50} and Δ_{s85} (i.e., same response, controlled by V_n).

3. MODEL VALIDATION AGAINST EXPERIMENTAL TESTS

The numerical model developed herein is calibrated by using the experimental tests described in Table 2. Two types of bare frames are considered to assess the reliability of the RC model, both in the case of ductile (BD) and non-ductile (BN) frames. To evaluate the infilled frames, three tests were selected: one non-ductile frame with a hollow brick panel (HN), one ductile frame with a solid brick panel (SD) and one non-ductile frame with a solid brick panel (SN). In the literature, no experimental tests with brittle failure of a ductile frame with hollow bricks were found. This is expected, considering the lower effect of hollow bricks and the higher shear performance of ductile frames. However, while the cyclic response of test SN has been simulated in many studies (e.g., Jeon et al. 2015), tests BN, HN, BD and SD have never been compared with cyclic numerical simulations.

Table 2. Details of the experimental tests selected for the model calibration.

Authors	ID	f_c [MPa]	scale	s [mm]	Brick type	τ_w [MPa]	t_w [mm]
Verderame et al. 2016	BN	21.6	1:2	150	Bare	-	-
Verderame et al. 2016	HN	22.7	1:2	150.0	Hollow Clay	0.36	80.0
Basha et al. 2016	BD	22.4	1:2	90.0	Bare	-	-
Basha et al. 2016	SD	22.4	1:2	90.0	Fly Ash Solid	0.14	110.0
Mehrabi et al. 1996	SN	26.8	1:2	63.5	Solid Clay	0.34	92.0

3.1 Shear failure in non-ductile and ductile RC bare models (BN and BD)

The gravity-load designed frame tested by Verderame et al. (Verderame et al. 2016), BN, was characterized by poor transverse reinforcement of columns to reproduce the behaviour of existing Italian buildings. The axial load during the quasi-static cyclic tests was equal to 10% of the capacity of the columns to simulate the presence of higher storeys in a five-storey building.

According to Verderame et al. (2016), the response of the frame under cyclic loading was characterized by first cracking at the beam ends, followed by diagonal cracking of the joints and flexural cracking of the columns. After the maximum strength was reached, a softening slope was observed in the hysteretic response envelope of the specimen due to major diagonal cracking in the beam-column joint, with shear failure of the joint occurring at the end of the test.

A comparison between the experimental results and the numerical simulation results is shown in Figures 7a and 7b. Failure in the finite element model was detected when the chord rotation limit was reached; the shear strength in the columns was lower than the shear strength capacity V_n. In Figure 7a, rotLim was assumed to be 0.036 (i.e., Δ_{s50}/L), which led to early shear failure of the column and an inaccurate simulation of the experimental backbone after this point. The relative difference between the energy dissipated in the numerical model (E_{DN}) and in the experimental test (E_{DE}) was also calculated as $\Delta E = (E_{DN}-E_{DE})/E_{DE}$. By assuming rotLim = Δ_{s50}/L, ΔE was calculated as -21%, while a closer match was obtained by increasing rotLim to Δ_{s80}/L (ΔE = +6%), as reported in Figure 7b.

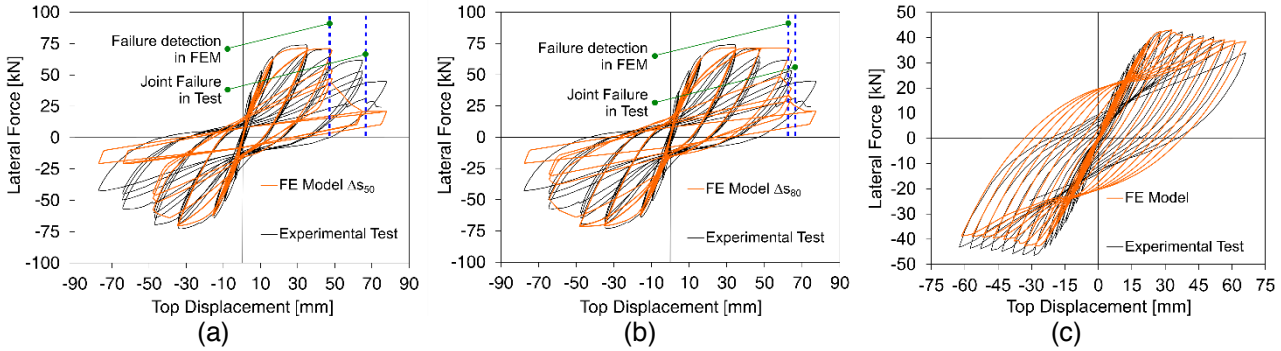

Figure 7. Numerical simulation of test BN adopting (a) Δs_{50} and (b) Δs_{80}, and test (c) BD (no shear failure).

A potential explanation of the mismatch between the test and simulation results in Figure 7a (i.e., adopting Δ_{s50} as rotLim) could be the different contribution in terms of deformability in the experimental test due to first cracking of the beam and the brittle shear failure of the joint. On the other hand, in the proposed model, the deformability of the beam-column joint is neglected, leading to higher chord rotation demand in the column for the attainment of the failure, compared to that identified in the experimental test; this difference was observed in other numerical simulations of non-ductile RC elements (e.g., Ghobarah and Biddha 1999; Youssef and Ghobarah 2001; Celik and Ellingwood 2008; Favvata et al. 2008; De Risi et al. 2017).

Despite the value of Δ_s adopted in the numerical model influences the results referred to the bare frame configuration, in the infilled model proposed in section 2.2, the shear failure of the column due to the local interaction with the infill is always obtained for drift levels substantially lower than Δ_{s50}/L, thus, the frame response after this value does not affect the numerical results. Furthermore, the numerical modelling of the joint response is crucial to avoid the failure occurring in the beam rather than in the joint (Favvata et al. 2008), while it is not as necessary when the focus is the brittle failure of the column due to local interaction. The inclusion of the joint for numerical modelling of infilled RC frames is an open challenge in the field and beyond the scope of this study, and *ad hoc* experimental results would be needed for calibration of the infill panel-joint interaction.

The bare specimen tested by Basha and Kaushik (2012; 2016), BD, was designed according to Indian standards for the highest seismic hazard zone. Confining reinforcement was increased in the critical zones of the beams and columns, adopting 90 mm spaced stirrups with 135° hooks. The vertical load was applied by placing concrete slabs on the beam to obtain an axial load equal to 1% of the capacity on each column. According Basha and Kaushik, the response to lateral loading of the frame was characterized by the formation of flexural cracks at the top of the columns, followed by minor shear crack development when drift increased. Finally, flexural failure of the columns was observed. The value of rotLim in this case is assumed to be 0.065 (i.e., Δ_{s50}/L).

The comparison between the numerical simulation and experimental results is provided in Figure 7c. The initial stiffness as well as the softening slope after the peak strength are accurately simulated by the numerical model; despite this fair agreement, the hysteresis loop comparison shows a difference, leading to a higher energy dissipation in the numerical model than in the experimental test (+26%). Shear failure is not detected in the numerical model (in compliance with the test observations), and the softening behaviour is due to the strength degradation of the concrete after the peak compressive strength and the cyclic compressive strength degradation of the longitudinal bars. This example effectively shows how the implemented model does not predict brittle failure in cases in which brittle failure does not occur.

3.2 Shear failure caused by hollow clay bricks (HN)

The infilled frame tested by Verderame et al. (2016), HN, is characterized by a masonry panel composed of hollow clay bricks, mostly used in the Mediterranean regions, with compressive strength equal to 4.88 and 3.19 MPa in the directions parallel and perpendicular to the holes, respectively. The diagonal tests conducted on the masonry determined a shear strength τ_w of 0.36 MPa. According to Verderame et al., the failure mode of the specimen was initially characterized by separation between the panel and the surrounding frame, followed by diagonal cracking of the infill and initial shear cracking at the top of the columns, corresponding to a drift equal to 0.50%. The post-peak behaviour of the specimen was characterized by increasing damage to the infill, and the test ended with brittle failure of the columns due to the widening of the shear cracks.

Referring to the results obtained from the numerical simulation, a significant reduction of lateral strength with respect to the experimental test is obtained in case of F_m/F_{cr} = 1.3 (Figure 8a), and the shear failure of the columns is not captured since the peak base shear of the test is not well-matched.

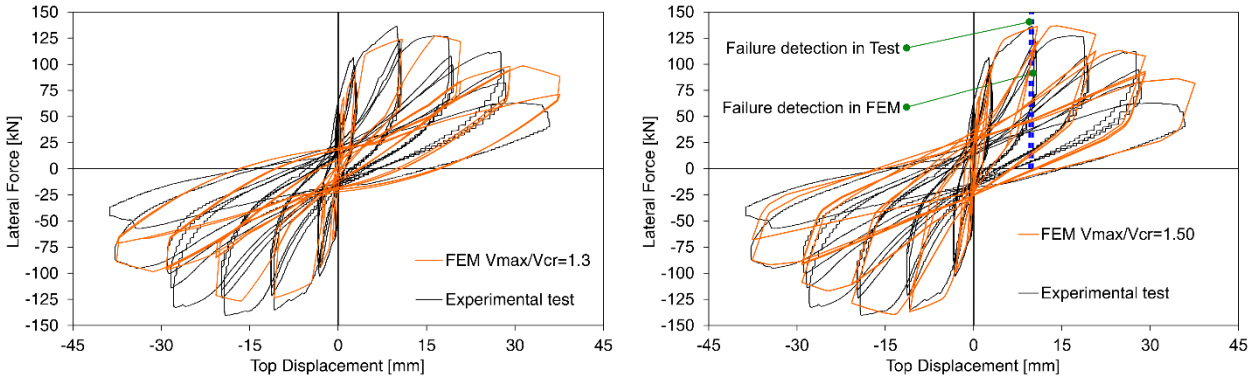

Figure 8. Numerical simulation of the test HN adopting (a) F_m/F_{cr} = 1.3 and (b) a three-strut model with F_m/F_{cr} = 1.50 (i.e., best experimental-numerical matching).

The best numerical-experimental matching is obtained by increasing the value of F_m up to $1.50F_{cr}$ (Figure 8b); shear failure of the column is obtained for the attainment of shear capacity at a drift value equal to 0.67% and a good correlation in terms of lateral strength and softening slope is observed.
A calibration of the hysteretic parameters of the *Pinching4* material was also conducted, to obtain a better match in terms of energy dissipation. rForce, rDisp and uForce were equal to 0.4, 0.3 and -0.15, respectively, while the reloading stiffness degradation limit was reduced to 0.2 (instead of the value 0.5 proposed by Kumar et al. (2015)). In this case, ΔE is +12%; emphasizing a very satisfactory capability of the model to capture the cyclic behaviour. The value of rotLim in this case (i.e., Δ_{s50}/L) is 0.047.

3.3 Shear failure caused by solid bricks (SD and SN)

The infilled frame tested by Basha and Kaushik (2012; 2016) had full-scale solid fly ash bricks with compressive strength equal to 5.7 MPa; the diagonal tests performed to define mechanical properties of the masonry showed a shear strength τ_w equal to 0.14 MPa and elastic modulus E_w equal to 2700 MPa.
According to Basha and Kaushik, the failure mode of the specimen was characterized by initial bed joint sliding of the infill at a drift level equal to 0.31%. By increasing the drift, diagonal cracks developed in the infills starting from the column ends. In the frame, flexural and shear cracks developed almost for the same value of drift (0.77%). The test was concluded at a drift equal to 4.62%, when shear cracks increased and spalling of concrete with subsequent buckling of longitudinal bars was observed.

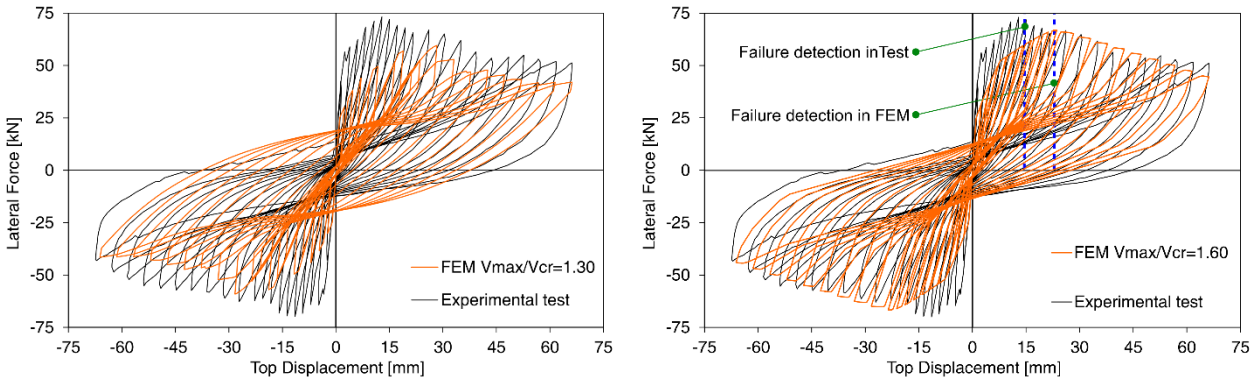

Figure 9. Numerical simulation of the SD test adopting (a) F_m/F_{cr} = 1.3 and (b) three-strut model with F_m/F_{cr} = 1.60 (i.e., best experimental to numerical matching).

Figure 9a shows a comparison between the numerical results obtained with the parameters proposed by Panagiotakos and Fardis for the evaluation of F_m and the experimental results. Considering a F_m/F_{cr} ratio equal to 1.3, the maximum lateral strength of the specimen is underestimated; moreover, in this case, the lower shear transferred to the column does not lead to shear failure of the columns. By increasing the F_m/F_{cr} ratio to 1.60 (Figure 9b), a closer match of the strength can be observed, and the shear failure of the columns is detected at a drift ratio of 1.35%. Referring to the three-strut model with F_m/F_{cr} equal to 1.60, the pinching effect is more significant due to the shear failure of the columns, more closely matching the experimental data. The original parameters adopted for rForce, rDisp and uForce were modified to 0.1, 0.8 and -0.15, respectively,

reducing the reloading stiffness degradation limit to 0.2 (same as section 3.2). Adopting these values, ΔE is equal to -3%. In this case, the value of rotLim was 0.065 (i.e., Δ_{s50}/L).
The infilled frame analysed by Mehrabi et al. (1996) is characterized by columns with low shear reinforcement, realized by adopting stirrups spaced 63 mm apart with 90° hooks; the masonry infill was composed of solid concrete bricks with a compressive strength of 13.85 MPa. The shear strength τ_w of the panel was equal to 0.35 MPa, and the elastic modulus E_w was 9165 MPa. The vertical load was applied both to the columns and beams, to obtain an axial load on each column equal to 35% of the axial load capacity.
According to Mehrabi et al., the failure mechanism was first characterized by diagonal cracking of the infill at a drift ratio of 0.33%; after the maximum lateral strength was reached, shear cracking of the column was observed, corresponding to a drift ratio of 1.32%. The test terminated at a drift ratio of 2.7%, after the development of shear cracking and ultimately crushing of the concrete in the columns.
Even in this case, the adoption of the ratio 1.3 between F_m and F_{cr} proposed by Panagiotakos and Fardis leads to a slight underestimation of the maximum lateral strength, as shown in Figure 10a. Although the numerical model matches the experimental results well during the first stage of the hysteretic response, the shear failure of the column is not obtained, and the softening slope is slightly higher in the numerical model.
For test SN, the best numerical-experimental matching is obtained by increasing the ratio F_m/F_{cr} to 1.45 (Figure 10b); the higher maximum strength of the infills leads to shear failure of the columns at a drift ratio of 1.23%, followed by a noticeable softening slope, which more accurately simulates the post-peak behaviour of the experimental test. The values of rForce, rDisp and uForce adopted to obtain the best match in terms of energy dissipation were equal to 0.4, 0.3 and -0.15 (as in test HN), reducing the stiffness degradation limit to 0.2 (as in all infilled tests considered in this study). In this case, the value of ΔE is +9%; the cause of this mismatch is the significant asymmetry of the hysteretic loops in the experimental test (Figure 10b). The value of rotLim assumed in this case is 0.048 (i.e., Δ_{s50}/L).

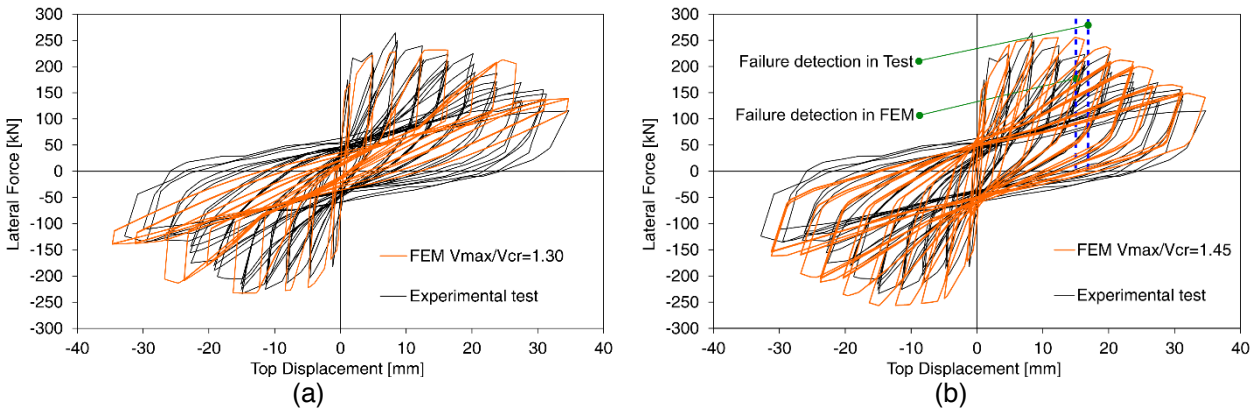

Figure 10. Numerical simulation of test SN adopting (a) F_m/F_{cr} = 1.3 and (b) a three-strut model with F_m/F_{cr} = 1.45 (i.e., best experimental-numerical matching).

Despite the modification of the hysteretic parameters of the *Pinching4* material with respect to the values proposed by Panagiotakos and Fardis and Kumar et al., no influence of these parameters on the column shear failure detection is observed for all the numerical simulation performed; the proposed values have been calibrated only to more accurately reproduce the hysteretic loops obtained from the experimental tests, and, consequently, the dissipated energy.

4. OVERSTRENGTH FACTORS AND SHEAR STRENGTH OF THE INFILL

The numerical simulations of the tests considered show a high sensitivity of the results to the ratio F_m/F_{cr} adopted for the definition of the force-displacement behaviour of the equivalent truss. An accurate matching of the peak response determines whether the brittle failure is identified. For each test considered, the original factor of 1.3, proposed by Panagiotakos and Fardis, is increased to obtain the best matching with the experimental results and to simulate the failure mode of the frame (i.e., shear failure). For all the tests considered in section 3, the brittle failure of the columns is not obtained by adopting the standard value of the overstrength; the correspondence between the experimental and numerical backbone curve envelope requires a higher value of F_m/F_{cr} (1.45-1.60, with an average of 1.51).
Based on the numerical simulations in section 3, an extended study is conducted on the overstrength factor, analysing the results obtained from a database of 98 experimental tests on masonry infilled RC frames, reported in Table 3 and selected from the database compiled by De Luca et al. (2016). The vast majority of the 98 tests considered included specimens in which no brittle failure in the column is observed (due to the

local interaction with the infill). The original database included two of the experimental tests (i.e., 100 tests in total) simulated in section 3; these tests are not considered herein to avoid the use of repetitive data for the validation of the numerical simulations in section 3. Using the 98 tests from the database, two distinct categories of frames and masonry panels were considered; the frames are defined as "ductile" or "non-ductile" depending on whether seismic criteria are adopted in the design, while the type of bricks adopted is considered to define the panel category as "solid" or "hollow".

The main mechanical and geometrical properties of the specimens characterizing the database range between the following values: 8.6 MPa≤f_c≤54.6 MPa; 0.0019≤ρ"≤0.02; 0.08 MPa≤τ_w≤1.07 MPa; 540 MPa≤E_w≤9528 MPa; 559 mm≤h_w≤2750 mm; 991 mm≤L_w≤4200 mm; 37.5 mm≤t_w≤300 mm.

Seven specimens featured central openings in the panel, while none of the tests were performed on infilled frames with eccentric openings. For most of the specimens, standard mortar joints were used to connect the panel to the frame; in 12 of the non-ductile frames with solid bricks specimens, steel plates were placed at the infill-frame interface and in one specimen of the non-ductile frames with solid bricks the connection was realized with dowel rebars.

De Luca et al. (2016) provided a piecewise linear fit of the positive and negative envelope of each test by assuming the optimization algorithm provided by De Luca et al. (2013). The fits obtained provided the global response of the frame and infill panel. Aimed at identifying the values of F_{cr} and F_m for the sole panel, the response of the frame is identified analytically and subtracted from the global piecewise linear fit. This approach does not depend on the assumption of the number of trusses employed to model the infill and is considered suitable to verify the trends in the overstrength observed from the numerical-experimental matching.

Referring to the presence of openings, several formulations are available in literature to modify the width of the equivalent strut depending on the presence of openings (Al-Chaar 2002; Furtado et al. 2018), resulting in a homothetic reduction to the main backbone. Consequently, this parameter does not influence the overstrength ratio. On the other hand, in case of eccentric openings, the stress distribution in the infill can significantly change (Kakaletsis and Karayannis 2007; Anić et al. 2017) and different modelling approaches are generally adopted to simulate the presence of the infill (FEMA 356 2000). For this reason, the results obtained from the present study do not cover the case of infilled frames with eccentric openings; further investigations need to be conducted, considering a wider database.

The lateral response of the frame is defined considering a bilinear hardening model. The lateral strength at the yielding point is defined as $V_y = 4 \cdot M_y/L$, where M_y and L are the yielding moment and the height of the column, respectively. The displacement at yielding D_y is obtained by multiplying the height of the column (L) and the chord rotation θ_y, evaluated according to Eurocode 8 Part 3 (EN 1998-3 2005). The ultimate lateral strength V_u is equal to $4 \cdot M_u/L$, where M_u is the ultimate moment evaluated from a fibre analysis of the section, while the corresponding ultimate displacement is evaluated as $D_u = L \cdot \theta_u$, where θ_u is the ultimate rotation, evaluated according to Eurocode 8 Part 3 (EN 1998-3 2005).

Table 3. Database of infilled frame tests.

Author	n. of tests	Frame typ.	Masonry bricks typ.
Kakaletsis et al. (2011)	12	Ductile	Hollow
Haris and Hortobágyi (2012)	11	Non-Ductile	Solid
Mehrabi et al. (1996)	13	Ductile (2) and Non-Ductile (10)	Hollow (7) and Solid (5)
Crisafulli et al. (2005)	2	Ductile (1) and Non-Ductile (1)	Solid
Colangelo (2003)	6	Ductile (4) and Non-Ductile (2)	Hollow
Colangelo (1996)	1	Ductile	Hollow
Colangelo (2005)	5	Non-Ductile	Hollow
Al-Chaar et al. (2002)	4	Non-Ductile	Hollow
Baran and Sevil (2010)	8	Non-Ductile	Hollow
Calvi and Bolognini (2001)	7	Ductile	Hollow
Al-Nimry (2014)	5	Non-Ductile	Solid
Di Trapani (2014)	12	Non-Ductile	Hollow (8) and Solid (4)
Basha and Kaushik (2016)	6	Ductile (2) and Non-Ductile (3)	Solid
Zovkić et al. (2013)	3	Ductile	Hollow
Piries and Carvalho (1992)	3	Ductile	Hollow
Skafida et al. (2014)	1	Non-Ductile	Hollow

The peak strength of the global backbone F_m is obtained before the failure (either flexural or shear) of the frame; thus, the simple bilinear model adopted is considered suitable for evaluating the overstrength ratio of the sole panel.

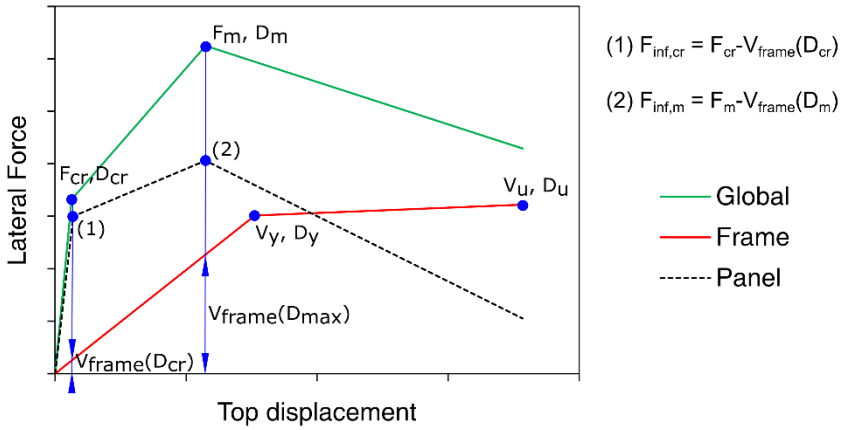

Figure 11. Evaluation of the *panel-only* backbone curve.

As shown in Figure 11, the strength at cracking $F_{inf,cr}$ and the maximum strength $F_{inf,m}$, characterizing the lateral response of the infill panel (herein referred to as the *panel-only* behaviour) are obtained by subtracting to the global strengths F_{cr} and F_m from the lateral strength of the frame at the displacements D_{cr} and D_m.
Referring to the global piecewise linear fit (i.e., the green line in Figure 11), the 98 values of overstrength are evaluated, and 84 usable values are obtained for the *panel-only* behaviour according to the procedure shown in Figure 11; in some cases, the evaluation of the overstrength of the single panel leads to non-convex shapes that are excluded considering that the subtracting procedure is unreliable for these tests.
To remove outliers, the data outside the range $\{Q_1-(Q_3-Q_1), Q_3+(Q_3-Q_1)\}$ are excluded, where Q_1 and Q_3 are the first and third quartiles of the sample, respectively. This final filtering resulted in 80 usable F_m/F_{cr} ratios.
The 80 values of F_m/F_{cr} for the panel are fitted according to a truncated log-normal distribution (Figure 12), considering 1.0 as the lower truncation limit. The basis for the truncation is the fact that the ratio between peak strength and the cracking strength of the infill has a physical limit to one as per definition of F_m and F_{cr}.
The median is 1.42, and standard deviation of the logarithm (β) is 0.20. This median value is higher than the results of the model by Panagiotakos and Fardis, confirming the observations of the numerical results, both for ductile and non-ductile frames as well as solid and hollow bricks. The median value obtained in this work is in line with the results by Burton and Deierlein (2013), who obtained a mean of 1.4 with a COV of 0.09. The overstrength distribution obtained emphasized that adapting the overstrength value of ± 0.1 is significant given the β of the distribution. By comparing the probability density functions obtained for the non-ductile frames with hollow and solid bricks (Figure 13), a noticeable difference in terms of the median value of the ratio F_m/F_{cr} is observed between the two distributions.

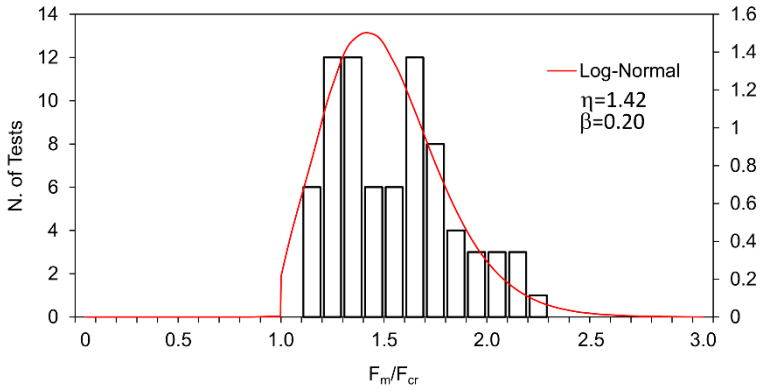

Figure 12. Log-normal distribution of the overstrength factors referring to the *panel-only* backbone.

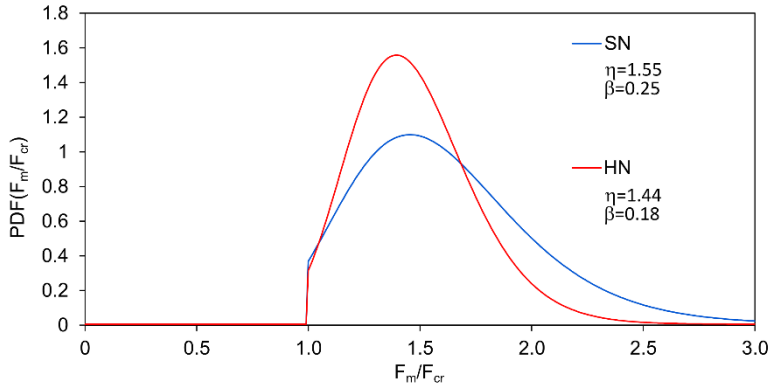

Figure 13. Probability density function of F_m/F_{cr} for non-ductile frames with hollow (red) and solid (blue) infills referring to *panel-only* backbone.

In both cases, the distributions of F_m/F_{cr} have higher mean values than the original model by Panagiotakos and Fardis. A total of 29 data points represents the case of non-ductile frames with hollow bricks (i.e., HN sample); these data have a median of 1.44, and $\beta = 0.18$. Additionally, 24 data points refer to the case of non-ductile frames with solid bricks (i.e., SN sample); for these data, the median is 1.55, and $\beta = 0.25$ (Figure 13). The case of ductile frames with solid bricks (i.e., SD sample) had only one value, 1.94; therefore, no distribution is available for this case.

Finally, a comparison between the probability density function obtained for the global system (infill + frame) and for the panel is provided in Figure 14. Referring to the global backbone curve, higher values of overstrength are generally obtained, with a mean value equal to 1.55, and $\beta = 0.20$. This overstrength value is expected to be higher because it also includes the RC frame contribution that, in many of the cases, is still in the increasing pre-yielding phase. For consistency, the same probability density function is adopted in the global backbone. It is worth noting that peak strength and cracking strength in panel-only and global do not necessarily correspond to the same loading step in the force-displacement envelope.

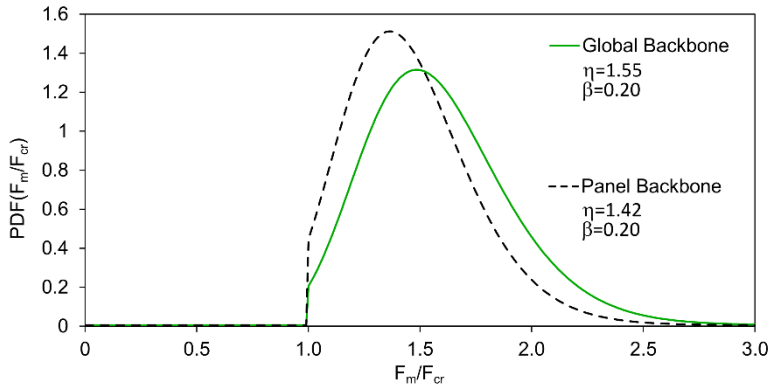

Figure 14. Comparison between the overstrength probability density function considering the global and *panel-only* backbone.

The results obtained through the metadata of the tests considered in the database are in accordance with the conclusions made in section 3, where for each test selected, the overstrength rate was increased to obtain the best matching with the experimental results and to capture the brittle failure.

According to the results obtained in this section, the median value of the overstrength obtained for the solid bricks is 1.55, which is close to 1.51. The value 1.51 is the average of 1.45 and 1.60, which are the overstrength employed in section 3 to match the two solid tests SD and SN (i.e., Basha and Kaushik 2016 and Mehrabi et al. 1996), respectively. The test SD is compared with the SN sample distribution, given the lack of data in the SD sample, considering that the type of infill (solid or hollow) is more influential on the evaluation of the overstrength factor. The values of 1.45 and 1.60, obtained in the numerical modelling in section 3, are the 39% and 55% percentiles of the SN distribution.

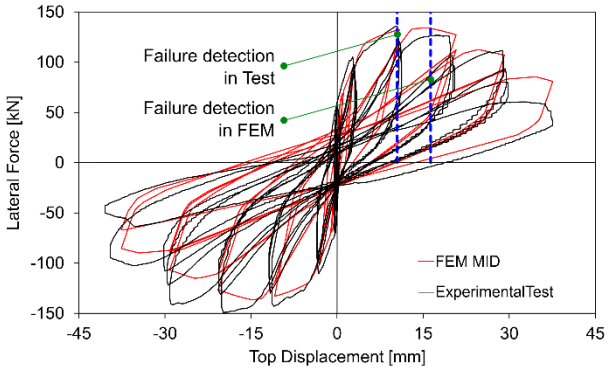

Figure 15. Numerical simulation of tests HN, adopting the median value obtained from the database for hollow bricks, namely, 1.44.

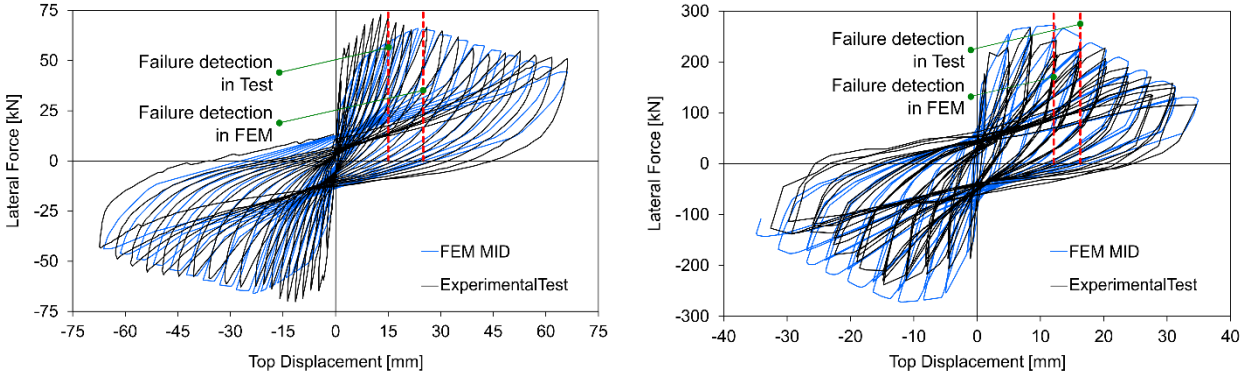

(a) (b)

Figure 16. Numerical simulation of tests (a) SD and (b) SN, adopting the median value obtained from the database for solid bricks, namely, 1.55.

For the test HN simulated (i.e., Verderame et al. 2016) the best matching value is 1.50, which is the 58% percentile of the HN distribution. Assuming the median values of the overstrength from the two distributions as obtained in Figure 13, namely, 1.44 for hollow bricks (Figure 15) and 1.55 for solid bricks (Figure 16a and 16b), would have captured the brittle failures in the tests even if the best possible numerical-experimental matching was not achieved as in Figures 8b, 9b and 10b. The values employed in Figure 15 and 16 can be recommended to be employed in predictive modelling of local interactions using three-strut macro-models.

5. CONCLUSIONS

The analysis of the local interaction between RC frames and masonry infills requires an accurate evaluation of the properties of both the panel and the frame members, through the adoption of models sufficiently accurate for simulating the complex nonlinear behaviour of the RC-infill system.

A novel combination of the consolidated three-strut macro-model for the panel with the recently developed *Pinching Limit State Material* for the RC members was adapted and proposed herein for analytically capturing the brittle failure of columns due to local interaction.

Experimental tests that exhibit brittle failure of a column were selected from the literature, considering specimens with hollow or solid infills and non-ductile or ductile RC frames. Two bare experimental tests (for the validation of the RC model) and three infilled tests were simulated through the novel modelling approach proposed. The cyclic behaviour of four of the five tests considered was numerically modelled for the first time. The numerical-experimental matching was optimized by adjusting the overstrength factor of the piecewise linear backbone of the infills (i.e., the ratio between the peak and cracking shear strength of the infill panel) and the hysteretic parameters of the infill model. The starting value was the well-consolidated and widely employed assumption of 1.3 suggested by Panagiotakos and Fardis. Aimed at capturing the brittle failure of the column, the optimal overstrength rate was increased, assuming values of 1.55, 1.45 and 1.60 for the hollow non-ductile, the solid non-ductile and the solid ductile tests, respectively. The trend of a higher overstrength

value from the model was also observed in other recent studies that did not focus on tests showing brittle failure.
The limited number of matching numerical-experimental simulations required a comparison with more general results related to a wider number of tests, regardless of the number of struts used in the numerical modelling. Therefore, a previously compiled database of 98 tests was considered and the overstrength factors of the panel were evaluated for each test and included as metadata through a simplified procedure. The distributions of the overstrength factor for the cases of hollow infills with non-ductile frames and solid infills with non-ductile frames were obtained and compared with the optimal values determined from the cyclic numerical simulations. The distribution for the case of solid infills with ductile frames was not evaluated, given the scarcity of the data for this category. The optimal values from the detailed numerical simulations corresponded to the 39%, 55% and 58% percentiles of the relevant distributions.
The results of the overstrength factor, provided by both the numerical simulations and the database comparison, suggested that the medians of the two distributions (namely, 1.44 for hollow non-ductile and 1.55 for solid non-ductile) can be confidently utilized in numerical modelling approaches aimed at the prediction of the occurrence of brittle failure in columns due to their local interaction with masonry infills.
Given the increasing availability of experimental tests, these results are not conclusive but represent a solid basis for improving the calibration of *ad hoc* overstrength coefficients for hollow and solid infills in numerical modelling aimed at the prediction of brittle failure caused by local interaction between infill and RC members. Further enhancements are needed to consider different infill materials and, in particular, two-layer hybrid configurations, which are currently more frequently used in the construction industry in compliance with building energy requirements.

ACKNOWLEDGEMENTS

This work was supported by the Royal Society International Exchange Scheme IE161016 “Cumulative damage of masonry infills caused by anthropogenic earthquakes” project. All the underlying data are provided in full within this paper.

REFERENCES

Al-Chaar, G. Evaluating strength and stiffness of unreinforced masonry infill structures. Rep. No. ERDC/CERL TR-02-1, 2002; U.S. Army Corps of Engineers, Champaign, Ill.

Al-Chaar G, Issa M, Sweeney S. Behavior of Masonry-Infilled Nonductile Reinforced Concrete Frames. Journal of Structural Engineering 2002; 128(8): 1055–1063.

Al-Nimry HS. Quasi-Static Testing of RC Infilled Frames and Confined Stone-Concrete Bearing Walls. Journal of Earthquake Engineering 2014; 18: 1–23.

Anić F, Penava D, Sarhosis V. Development of a three-dimensional computational model for the in-plane and out-of-plane analysis of masonry-infilled reinforced concrete frames. COMPDYN 2017 - Proceedings of the 6th International Conference on Computational Methods in Structural Dynamics and Earthquake Engineering. Rhodes Island, Greece, 2017.

ASCE/SEI 41-13. Seismic evaluation and retrofit of existing buildings. American Society of Civil Engineers; 2014.

Asteris PG, Antoniou ST, Sophianopoulos DS, Chrysostomou CZ. Mathematical Macromodeling of Infilled Frames: State of the Art. Journal of Structural Engineering 2011; 137(12): 1508–1517.

ASTM E 519-02. Standard Test Method for Diagonal Tension (Shear) in Masonry Assemblages. American Society for Testing Materials 2002.

Axley JW, Bertero, VV. Infill panels: their influence on seismic response of buildings 1979; 79(28), University of California, Berkeley.

Baran M, Sevil T. Analytical and experimental studies on infilled RC frames. International Journal of the Physical Sciences 2010; 5(13): 1981–1998.

Basha SH, Kaushik HB. Evaluation of Shear Demand on Columns of of Masonry Infilled Reinforced Concrete Frames. Proceedings of the 15th World Conference on Earthquake Engineering, Lisbon (PT), 2012.

Basha SH, Kaushik HB. Behavior and failure mechanisms of masonry-infilled RC frames (in low-rise buildings) subject to lateral loading. Engineering Structures 2016; 111: 233–245.

Bertoldi SH, Decanini LD. Telai tamponati soggetti ad azioni sismiche - un modello semplificato: confronto

sperimentale e numerico. 6° Convegno nazionale l'ingegneria sismica in Italia, 1993.

Burton H, Deierlein G. Simulation of Seismic Collapse in Non-Ductile Reinforced Concrete Frame Buildings with Masonry Infills. Journal of Structural Engineering 2013; 140(8): A4014016.

Calvi GM, Bolognini D. Seismic Response of Reinforced Concrete Frames Infilled With Weakly Reinforced Masonry Panels. Journal of Earthquake Engineering 2001; 5(2): 153–185.

Cavaleri L, Di Trapani F. Cyclic response of masonry infilled RC frames: Experimental results and simplified modeling. Soil Dynamics and Earthquake Engineering 2014; 65: 224–242.

Çelebi M, Bazzurro P, Chiaraluce L, Clemente P, Decanini L, Desortis A, et al. Recorded motions of the 6 April 2009 Mw6.3 L'Aquila, Italy, earthquake and implications for building structural damage: Overview. Earthquake Spectra 2010; 26(3): 651–684.

Celik OC, Ellingwood BR. Modeling beam-column joints in fragility assessment of gravity load designed reinforced concrete frames. Journal of Earthquake Engineering 2008; 12(3): 357–381.

Chrysostomou CZ. Effects of degrading infill walls on the nonlinear seismic response of two-dimensional steel frames. PhD Thesis, Cornell University, 1991.

Chrysostomou CZ, Gergely P, Abel JF. A six-strut model for nonlinear dynamic analysis of steel infilled frames. International Journal of Structural Stability and Dynamics 2002; 2(3): 335–353.

Chrysostomou CZ, Asteris PG. On the in-plane properties and capacities of infilled frames. Engineering Structures 2012; 41: 385–402.

Colangelo F. Pseudodynamic tests on brick-infilled RC frames. 11th World Conference on Earthquake Engineering, Acapulco (MX), 1996.

Colangelo F. Experimental Evaluation of Member-By-Member Models and Damage Indices for Infilled Frames. Journal of Earthquake Engineering 2003; 7(1): 25–50.

Colangelo F. Pseudo-dynamic seismic response of reinforced concrete frames infilled with non-structural brick masonry. Earthquake Engineering and Structural Dynamics 2005; 34(10): 1219–1241.

Comité Euro-international du Béton, CEB. RC frames under earthquake loading: state of the art report 1996 (Vol. 231). Thomas Telford.

Crisafulli FJ. Seismic behaviour of reinforced concrete structures with masonry infills. PhD thesis, University of Canterbury, New Zealand, 1997.

Crisafulli FJ, Carr AJ. Proposed macro-model for the analysis of infilled frame structures. Bulletin of the New Zealand Society for Earthquake Engineering 2007; 40(2): 69–77.

Crisafulli FJ, Carr AJ, Park R. Experimental response of framed masonry structures designed with new reinforcing details. Bulletin of the New Zealand Society for Earthquake Engineering 2005; 38(1): 19–32.

De Luca F, Vamvatsikos D, Iervolino I. Near-optimal piecewise linear fits of static pushover capacity curves for equivalent SDOF analysis. Earthquake Engineering and Structural Dynamics 2013; 42: 523–543.

De Luca F, Verderame GM, Gómez-Martínez F, Pérez-García A. The structural role played by masonry infills on RC building performances after the 2011 Lorca, Spain, earthquake. Bulletin of Earthquake Engineering 2014; 12(5): 1999–2026.

De Luca F, Morciano E, Perrone D, Aiello MA. MID 1.0: Masonry Infilled RC Frame Experimental Database. Italian Concrete Days 2016, Rome, Italy, 27-28 October 2016 (DOI: 10.1007/978-3-319-78936-1_11).

De Luca F, Woods GED, Galasso C, D'Ayala D. RC infilled building performance against the evidence of the 2016 EEFIT Central Italy post-earthquake reconnaissance mission: empirical fragilities and comparison with the FAST method. Bulletin of Earthquake Engineering 2017: 1–27 (DOI: 10.1007/s10518-017-0289-1).

Decanini LD, De Sortis A, Goretti A, Liberatore L, Mollaioli F, Bazzurro P. Performance of Reinforced Concrete Buildings During the 2002 Molise, Italy, Earthquake. Earthquake Spectra 2004; 20(S1): S221–S255.

De Risi MT, Ricci P, Verderame GM. Modelling exterior unreinforced beam-column joints in seismic analysis of non-ductile RC frames. Earthquake Engineering and Structural Dynamics 2017; 46: 899–923.

Dhakal RP, Maekawa K. Path-dependent cyclic stress – strain relationship of reinforcing bar including buckling.

Engineering Structures 2002; 24: 1383–1396.

Di Trapani F. Masonry infilled RC frames: Experimental results and development of predictive techniques for the assessment of seismic response. PhD thesis, Università degli Studi di Palermo, 2014.

Dolšek M, Fajfar P. Soft storey effects in uniformly infilled reinforced concrete frames. Journal of Earthquake Engineering 2001; 5(1): 1–12.

Dolšek M, Fajfar P. Simplified non-linear seismic analysis of infilled reinforced concrete frames. Earthquake Engineering and Structural Dynamics 2005; 34(1): 49–66.

Dolšek M, Fajfar P. The effect of masonry infills on the seismic response of a four-storey reinforced concrete frame - a deterministic assessment. Engineering Structures 2008; 30(7): 1991–2001.

El-Dakhakhni WW, Elgaaly M, Hamid AA. Three-Strut Model for Concrete Masonry-Infilled Steel Frames. Journal of Structural Engineering 2003; 129(2): 177–185.

Elwood KJ. Modelling failures in existing reinforced concrete columns. Canadian Journal of Civil Engineering 2004; 31(5): 846–859.

Elwood KJ, Moehle JP. Drift Capacity of Reinforced Concrete Columns with Light Transverse Reinforcement. Earthquake Spectra 2005; 21(1): 71–89.

Elwood KJ, Eberhard MO. Effective Stiffness of Reinforced Concrete Columns. ACI Structural Journal 2009; 106(4): 476-484.

EN 1996-3. Eurocode 6 - Design of masonry structures - Part 3: Simplified calculation methods for unreinforced masonry structures. European Standard, 2006.

EN 1998-1. Eurocode 8: Design of structures for earthquake resistance – Part 1: General rules, seismic actions and rules for buildings. European Standard, 2004.

EN 1998-3. Eurocode 8: Design of structures for earthquake resistance - Part 3: Assessment and retrofitting of buildings. European Standard, 2005.

Favvata MJ, Izzuddin BA, Karayannis CG. Modelling exterior beam–column joints for seismic analysis of RC frame structures. Earthquake Engineering and Structural Dynamics 2008; 37(13): 1527–1548.

FEMA 274. NEHRP Commentary on the Guidelines for the seismic rehabilitation of buildings. Federal Emergency Menagement Agency: 1997.

FEMA 306. Evaluation of earthquake damaged concrete and masonry wall buildings. Federal Emergency Management Agency: 1998.

FEMA 356. Prestandard and Commentary for the Seismic Rehabilitation of Building. Federal Emergency Menagement Agency: 2000.

Furtado A, Rodrigues H, Arêde A. Calibration of a simplified macro-model for infilled frames with openings. Advances in Structural Engineering 2018; 21(2): 157–170. DOI: 10.1177/1369433217713923.

Ghobarah A, Biddah A. Dynamic analysis of reinforced concrete frames including joint shear deformation. Engineering Structures 1999; 21(11): 971–987.

Hak S, Morandi P, Magenes G, Sullivan TJ. Damage Control for Clay Masonry Infills in the Design of RC Frame Structures. Journal of Earthquake Engineering 2012; 16(sup1): 1–35.

Haris I, Hortobágyi Z. Comparison of experimental and analytical results on masonry infilled RC frames for monotonic increasing lateral load. Periodica Polytechnica Civil Engineering 2012; 56(2): 185–196.

Jeon JS, Park JH, DesRoches R. Measuring bias in structural response caused by ground motion scaling. Earthquake Engineering and Structural Dynamics 2015; 44: 1783–1803.

Kakaletsis, DJ., & Karayannis, CG. Experimental investigation of infilled r/c frames with eccentric openings. Structural Engineering and Mechanics 2007; 26(3), 231-250.

Kakaletsis, DJ., & Karayannis, CG. Influence of masonry strength and openings on infilled R/C frames under cycling loading. Journal of Earthquake Engineering 2008; 12(2), 197-221.

Kakaletsis DJ, David KN, Karayannis CG. Effectiveness of some conventional seismic retrofitting techniques for bare and infilled R/C frames. Structural Engineering and Mechanics 2011; 39(4): 499–520.

Kose MM. Parameters affecting the fundamental period of RC buildings with infill walls. Engineering Structures 2009; 31(1): 93–102.

Kumar, M., Rai, D. C., & Jain, S. K. Ductility reduction factors for masonry-infilled reinforced concrete frames. Earthquake Spectra 2015; 31(1), 339-365.

Leborgne MR, Ghannoum WM. Analytical Element for Simulating Lateral-Strength Degradation in Reinforced Concrete Columns and Other Frame Members. Journal of Structural Engineering 2014; 140(7): 4014038.

Lowes, L. N., Mitra, N., and Altoontash, A. A beam-column joint model for simulating the earthquake response of reinforced concrete frames. Technical Rep. No. PEER 2003/10, 2003, PEER, Berkeley, California.

Mainstone RJ. On the stiffnesses and strengths of infilled frames. Proceedings of the Institution of Civil Engineers 1971; 49(2): 57–90.

Mander JB, Priestley MJ, Park R. Theoretical stress–strain model for confined concrete. Journal of Structural Engineering 1988; 114(8): 1804–1826.

Manfredi G, Prota A, Verderame GM, De Luca F, Ricci P. 2012 Emilia earthquake, Italy: reinforced concrete buildings response. Bulletin of Earthquake Engineering 2014; 12(5): 2275–2298.

McKenna F, Fenves GL, Scott MH, Jeremir B. Open system for earthquake engineering simulation, OpenSEES. University of Berkeley; 2000.

Mehrabi, A. B., Shing, P. B., Schuller, M. P., & Noland, J. L. Performance of masonry-infilled R/C frames under in-plane lateral loads. 1994, Rep. CU/SR-94, 6.

Mehrabi AB, Shin PB, Schuller MP, Noland JL. Experimental Evaluation of Masonry In-filled RC frames. Journal of Structural Engineering 1996; 122(3): 228–237.

Nakamura T, Yoshimura M. Gravity Load Collapse of Reinforced Concrete Columns with Brittle Failure Modes. Journal of Asian Architecture and Building Engineering 2002; 1(1): 21–27.

Ning N, Yu D, Zhang C, Jiang S. Pushover Analysis on Infill Effects on the Failure Pattern of Reinforced Concrete Frames. Applied Sciences 2017; 7(4): 428.

Noh NM, Liberatore L, Mollaioli F, Tesfamariam S. Modelling of masonry infilled RC frames subjected to cyclic loads: State of the art review and modelling with OpenSees. Engineering Structures 2017; 150: 599–621.

Panagiotakos TB, Fardis MN. Seismic Response of Infilled RC Frame Structures. 11th World Conference on Earthquake Engineering, June 23-28, Acapulco, MX: 1996.

Parisi F, De Luca F, Petruzzelli F, De Risi R, Chioccarelli E. Field inspection after the May 20th and 29th 2012 Emilia-Romagna earthquakes. Available at http://www.reluis.it: 2012.

Perrone D, Saponaro V, Leone M, Aiello M. Influence of Masonry Infills on the Shear Forces of RC Framed Structures. Applied Mechanics and Materials 2016; 847: 361-368.

Perrone D, Leone M, Aiello MA. Non-linear behaviour of masonry infilled RC frames: Influence of masonry mechanical properties. Engineering Structures 2017; 150: 875–891.

Pires F, Carvalho EC. The behaviour of infilled concrete frames under horizontal cyclic loading. Earthquake Engineering, tenth World Conference, Balkema, Rotterdam: 1992.

Polyakov SV. On the interaction between masonry filler walls and enclosing frame when loading in the plane of the wall. San Francisco: 1960.

Pujol S, Fick D. The test of a full-scale three-story RC structure with masonry infill walls. Engineering Structures 2010; 32(10): 3112–3121.

Reza M, Kakavand A. Limit State Material Manual. School of Civil Engineering, College of Engineering, University of Tehran, Iran, 2009.

Ricci P, De Risi MT, Verderame GM, Manfredi G. Procedures for calibration of linear models for damage limitation in design of masonry-infilled RC frames. Earthquake Engineering and Structural Dynamics 2016; 45(8): 1315–1335.

Sassun K, Sullivan TJ, Morandi P, Cardone D. Characterising the in-Plane Seismic Performance of Infill Masonry. Bulletin of the New Zealand Society for Earthquake Engineering 2016; 49(1): 100–117.

Sezen H, Whittaker AS, Elwood KJ, Mosalam KM. Performance of reinforced concrete buildings during the August 17, 1999 Kocaeli, Turkey earthquake, and seismic design and construction practise in Turkey. Engineering Structures 2003; 25(1): 103–114.

Sezen H, Moehle JP. Shear Strength Model for Lightly Reinforced Concrete Columns. Journal of Structural Engineering 2004; 130(11): 1692–1703.

Skafida S, Koutas L, Bousias SN, Skafida S, Koutas L, Bousias SN. Analytical Modeling of Masonry Infilled RC Frames and Verification with Experimental Data. Journal of Structures 2014; 2014: 1–17.

Stafford Smith B, Carter C. A method of Analysis for Infilled Frames. Proceedings of the Institution of Civil Engineers 1969; 44(1): 31–48.

Stavridis A, Shing PB. Finite-Element Modeling of Nonlinear Behavior of Masonry-Infilled RC Frames. Journal of Structural Engineering 2010; 136(3): 285–296.

Uva G, Porco F, Fiore A. Appraisal of masonry infill walls effect in the seismic response of RC framed buildings: A case study. Engineering Structures 2012; 34: 514–526.

Varum, H., Rodriguez, H., and Costa, A. Numerical Model to Account for the Influence of Infill Masonry on the RC Structures Behaviour, 2005, Proceedings of XII Portuguese Society Meeting/III International Material Symposium, University of Aveiro, Portugal.

Verderame GM, De Luca F, Ricci P, Manfredi G. Preliminary analysis of a soft-storey mechanism after the 2009 L'Aquila earthquake. Earthquake Engineering and Structural Dynamics 2011; 40(8): 925–944.

Verderame GM, Ricci P, Del Gaudio C, De Risi MT. Experimental tests on masonry infilled gravity- and seismic-load designed RC frames. 16th International Brick and Block Masonry Conference, Padova (IT): 2016.

Youssef M, Ghobarah A. Modelling of RC beam-column joints and structural walls. Journal of Earthquake Engineering 2001; 5(1): 93–111.

Zhu, L., Elwood, K. J., & Haukaas, T. (2007). Classification and seismic safety evaluation of existing reinforced concrete columns. Journal of Structural Engineering, 133(9), 1316-1330.

Zovkić J, Sigmund V, Guljas I. Cyclic testing of a single bay reinforced concrete frames with various types of masonry infill. Earthquake Engineering and Structural Dynamics 2013; 42: 1131–1149.